Journal of Materials Chemistry B

Accepted Manuscript

ROYAL SOCIETY OF CHEMISTRY

www.rsc.org/materialsB

Journal of Material Chemistry B

RSCPublishing

ARTICLE

Hexagonal Magnetite Nanoprisms: Preparation, Characterization and Cellular Uptake

Cite this: DOI: 10.1039/xoxxoooooox

Received ooth January 2012,
Accepted ooth January 2012

DOI: 10.1039/xoxxoooooox

www.rsc.org/

H. Wang [a], T. B. Shrestha[b], M. T. Basel[b], M. Pyle[b], Y. Toledo [a], A. Konecny [a], P. Thapa[c], M. Ikenberry[d], K. L. Hohn[d], V. Chikan [a], D. L. Troyer[b] and S. H. Bossmann[a]

The capacity of iron oxide nanocrystals to heat tissue when subjected to an alternating magnetic field (AMF hyperthermia) is shape-selective. Although iron oxide nanostructures with numerous shapes have been synthesized to date, hexagonal Fe_3O_4 prisms of low toxicity remained elusive. Here, we report the use of a dual ligand system permitting feasible reaction conditions to synthesize nearly perfect hexagonal Fe_3O_4 nanoplatelet structures, with edge length of 45 +/- 5 nm and thickness of 5 to 6 nm. Their Specific Absorption Rate (SAR) is > 750 $Wg(Fe)^{-1}$. The Fe_3O_4 hexagons were coated with a dopamine-based ligand to increase dispersibility in aqueous buffers. The Fe_3O_4 hexagons were only minimally toxic to RAW264.7 cells, which can be utilized in cell-based cancer targeting approaches.

1. Introduction

Magnetic iron oxide nanocrystals have attracted immense attention due to their versatile applications including high-density data storage,[1] contrast enhancement agents for magnetic resonance imaging (MRI),[2] ferrofluids,[3] drug delivery carriers,[4] bioprobes[5] and catalysis.[6] Iron oxide with various shapes such as spheres,[7] cubes,[8] worms,[9] stars,[10] rods,[11] octahedrons,[12] diamonds and prisms[13] have been synthesized successfully to date. The electric and magnetic properties of iron oxide have been demonstrated to be highly shape-dependent. For instance, Zhen *et al.* reported that the relaxivity of cubic iron oxide nanoparticles is four times higher than of their spherical counterparts.[14] Salazar-Alvarez *et al.* found that spherical maghemite nanoparticles exhibit a larger blocking temperature (T_B) than cubic maghemite nanoparticles.[15] Recently, Martinez-Boubeta *et al.* demonstrated that single-domain cubic iron oxide shows a superior magnetic heating efficiency, compared to spherical particles of similar sizes.[16] Despite the success achieved in shape-controlled methodology, nanoscale iron oxide with a hexagonal morphology is still very rare. Li *et al.* synthesized hexagonal nanoplatelets of Fe_3O_4 in supercritical CO_2 under high pressure with temperature ranging between 650-750 ^oC.[17], but a reliable synthesis at normal pressure and modest reaction temperatures, which can easily be scaled up, had not yet been reported.

Here, we report the synthesis of hexagonal magnetite (Fe_3O_4) nanoplatelets (HMNPs) by thermal decomposition of iron(III) acetylacetonate ($Fe(acac)_3$). The HMPNs are taken up well by defensive cells (monocyte/macrophage-like cells, RAW264.7) and possess very high Specific Absorption Rates in A/C-magnetic fields, making them suitable nanoparticles for cell-based hyperthermia treatment of cancer.

2. Materials and Methods

2.1. Preparation of Hexagonal Fe_3O_4 Nanoplatelets

0.71 g of $Fe(acac)_3$ was added to a mixture of 1.27 g of oleic acid and 0.5 g of stearic acid in 10.4 g of benzyl ether. After degassing at room temperature for 1 hour with Ar, the reaction mixture was heated to 290 ^oC at the rate of 20 ^oC/min under vigorous stirring. The reaction mixture was maintained at 290 ^oC for 30 min, and then cooled to room temperature naturally. The resulted mixture was diluted with 10 mL hexane and 30 mL toluene. The nanoparticles were collected by centrifugation (2000 RPM) and washed with chloroform three times.

The coating of the Fe_3O_4 nanoplatelets with the dopamine stealth ligand and the characterization techniques used, are described in the SI section.

2.2 IMAGE Analysis

The TEM data was analyzed using the program IMAGE, generously provided by the National Institutes of Health (www.NIH.gov/IMAGE).

2.3 Powder X-ray diffraction (XRD) patterns were obtained on a Bruker D8 X-ray diffractometer with Cu Kα radiation.

2.4 X-ray photoelectron spectroscopy (XPS) data was obtained with a Perkin-Elmer PHI 5400 electron spectrometer using acrochromatic Al Kα radiation (1486.6 eV) and a analyzer pass energy of 17.9 eV

2.5 Zeta potential measurements were performed using ZetaPALS Zeta Potential Analyzer purchased by Brookhaven Instruments Corporation.[18] The HMNPs were characterized in 1 X PBS at 298K. Their concentration was 0.1mg/mL.

2.6 AMF Heating of Hexagonal Fe_3O_4 Nanoplatelets

A copper coil (diameter 1 inch, 4 turns) coupled with 5 kA/m field amplitude, (Superior Induction Company, Pasadena, CA) was used to generate 366 kHz sinusoidal alternating magnetic field (AMF). The coil was coated with silver and cooled with circulating DI water to eliminate residual heating effects from the resistive loss. 1 mL colloidal solution of 5 in DI water (1 mg/mL) and 1 mL of DI water were subjected to AMF. The temperature was monitored by fiber optic probe (Neoptix, Quebec, Canada). The specific absorption rate (SAR) was calculated by the following equation [19]:

$$SAR = C\frac{\Delta T}{\Delta t}\frac{1}{m_{mag}}$$

Where C is the specific heat of solvent (C_{water} = 4.18 J g^{-1} ^oC), $\Delta T/\Delta t$ is the initial slope of the time-dependent temperature curve and m_{mag} is the weight fraction of magnetic element (Fe) in the sample.

2.6 HMNPs Cell Loading, and Cell Lifting Procedure

Raw 264.7 (Mo/Ma) cells were plated in 12 well plates at a density of 100,000 cells/cm^2. Once the cells were attached, the medium was removed and 1 mL medium containing different concentrations of HMNPs (0-50 μg/mL) was added in each well and incubated for 24 hours. The medium was collected in a 15 mL tube and the cells were washed with 1 X PBS (1mL). The supernatant was collected in a tube containing 1 mL of ice-cold 0.5 % EDTA in 1 X PBS. This solution was added to each well and incubated for 30 min at 0 ^oC. Then the attached cells were dislodged by pipetting repeatedly using 1 mL of this solution. The dislodged cells were collected in a tube containing medium, then rinsed, and centrifuged for 3 min at 1000 rpm. The supernatant was aspirated and the resulting cell pellet was suspended in 1 ml 1 X PBS. Live vs. dead cells were counted in hemocytometer with trypan blue exclusion dye. (1:1 cell suspension: trypan blue).[20] Each hemocytometer half was photographed with the Moticam 2500 on an upright scope. These photographs were then used to obtain cell counts.

3. Results and Discussion

3.1 HMNPs Synthesis and Characterization

We employed a mixture of two capping ligands under relatively mild conditions. Shape selectivity is achieved during growth by this "dual ligand system". Hyeon *et al.* reported the synthesis of uniform magnetite nanocubes with size ranging from 20 to 160 nm.[8b] We further developed this method by introducing stearic acid as second ligand and obtained hexagonal magnetite (Fe_3O_4) nanoplatelets. In a typical example, 0.71 g of $Fe(acac)_3$ was added to a mixture of 1.27 g of oleic acid and 0.5 g of stearic acid in 10.4 g of benzyl ether. After degassing at room temperature for 1 hour, the reaction mixture was heated to 290 ^oC at the rate of 20 ^oC/min under vigorous stirring. The reaction mixture was maintained at 290 ^oC for 30 min, and then allowed to cool to room temperature. The nanoparticles were collected by centrifugation (5,000 RPM) and further washed with chloroform.

TEM imaging (Figure 1A) reveals that over 85% of synthesized nanoparticles are hexagonal. High-resolution TEM (HRTEM) imaging of a series of representative nanocrystals (Figure 1B) demonstrates a near perfect hexagonal nanoplatelet structure, with edge length of 45 nm, and thickness of 5 to 6 nm, estimated from the "shadow" of the edge (Figure 1C). Further magnification (Figure 1D) reveals that these nanoparticles are single crystalline face-centered cubic (fcc) Fe_3O_4, as demonstrated by their atomic lattice fringes.

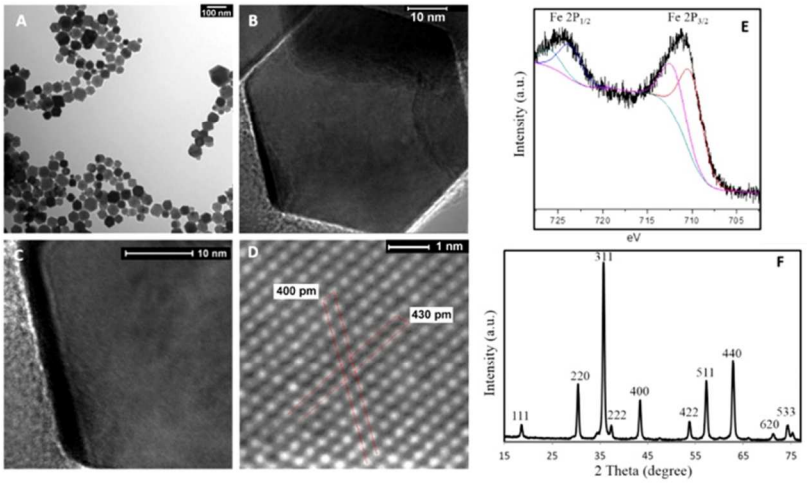

Figure 1. TEM and HRTEM of hexagonal Fe_3O_4 nanoplatelets A) TEM of nanoplatelets, B) HRTEM of a representative hexagonal nano-platelet, C) HRTEM side-view of the depth of the nanoplatelet, D) HRTEM of monocrystalline hexagonal nanoplatelet. The (111) planes of the iron bcc crystal structure are highlighted. E) XPS spectrum of iron oxide (Fe_3O_4) nanoplatelets. F) XRD patterns of iron oxide (Fe_3O_4) nanoplatelets.

The lattice spacing is about 0.4 nm, which can be assigned to the {111} plane of Fe_3O_4. The X-ray photoelectron spectroscopic (XPS) characterization (Figure 1E) shows binding energy peaks at 711.2 and 724.7 eV, which are in good agreement with the known values for Fe $2p_{3/2}$ and Fe $2p_{1/2}$ of magnetite,

respectively.[21] X-ray diffraction (XRD) analysis (Figure 1F) confirms the high crystalline nature of the material: 10 clear diffraction peaks can be assigned to the (111), (220), (311), (222), (400), (422), (511), (440), (622), (533) crystal faces of the cubic phase magnetite.[22]

3.2 Formation Mechanism of Nanoplatelets

Based on HRTEM analysis, Hyeon *et al.* have established a kinetic paradigm for growing Fe_3O_4 nanocubes from iron(III) acetylacetonate utilizing oleic acid.[8b] Nanocubes are formed as a result of faster growth along {111} than {100} directions, because oleic acids bind stronger to {100} planes. However, this paradigm is unable to fully explain why hexagonal prisms can be formed during crystal growth. In fcc Fe_3O_4, the surface energy of {111} surfaces is lowest, followed by {100}, whereas {110} is highest.[21,23] Therefore, if thermodynamics would determine the pattern of crystal growth, octahedral or tetrahedral structures featuring only {111} planes would be obtained. Whereas high-energy {110} Fe_3O_4 surfaces have been explored in catalysis[23], low energy {111} surfaces are required for biological/medicinal applications, because reactions with proteins have to be kept to a minimum. Li *et al.* have shown that anisotropic morphologies of fcc Fe_3O_4 can be directed by the formation of twin planes on {111}-type facets.[24] Directed by the six-fold symmetry of fcc crystal lattices, these twinned crystals form hexagonal-shaped nuclei. The presence of stearic acid in the system apparently lowers the stacking fault energy, causing > 85 percent of the Fe_3O_4 nuclei to form twin planes. Growth then proceeds at the resulting six surfaces in the x,y plane. It is noteworthy that the stacking faults of these twin planes cause {111} faces to form in alternating concave and convex orientations.[24] Crystal growth in the z-direction can be achieved when a hexagonal-shaped nucleus attaches itself to the {111} plane at the top of bottom of the (nano)crystal (Scheme 1). The proposed growth mechanism is evidenced by the findings reported in Figures 2 and 5A: a minor fraction of the hexagonal nanoplatelets is significantly smaller (50-70nm in diameter) than the main fraction (85-100nm). This can be regarded as proof that the hexagonal nanoplatelets first take shape and then grow at their surfaces in the x,y plane.

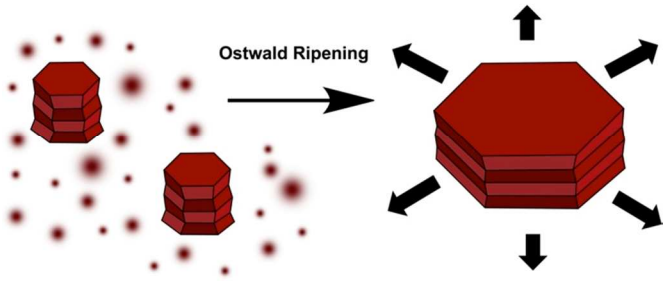

Scheme 1. Hexagonal Magnetic Nanoprisms (HMNPs) are formed in two steps: Among other precursor nanoparticles, hexagonal-shaped nuclei are formed by means of twinning on {111}-type facets. Size evolution then occurs via Ostwald ripening.

3.3 Enhancing the Biocompatibility of HMNPs via Ligand Exchange

Scheme 2 illustrates our synthetic approach towards both, water solubility and biocompatibility of the hexagonal magnetite prisms.[4d] The reaction sequence, starting from dopamine, requires six steps for the attachment of tetraethylene glycol. The octanol/water partition coefficient log P is -0.54 for ligand **4**.[25] Due to the strong binding affinity of dopamine to iron oxide[26], reacting the hexagonal magnetite prisms with ligand **4** in 1/1 methanol/chloroform (v/v) for 12 hours yields water-soluble HMNPs **5**. The water solubility of the ligand coated HMNPs is 5.8 ± 0.7mg/mL at 300K, and the zeta potential is -51 ± 1.3 mV in PBS.[18]

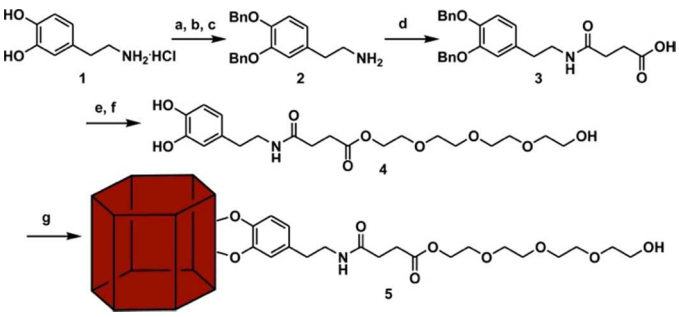

Scheme 2. Conditions: (a) triethyl amine, tert-butyl dicarbonate, CH_3OH, 12h; (b) BnBr, K_2CO_3, DMF, rt, 24 h; (c) 10% CF_3COOH, CH_2Cl_2, rt, 5 h; (d) succinic anhydride, pyridine, rt, 3 h; (e) EDC, DMAP, tetraethylene glycol, CH_2Cl_2, 12h; (f) Pd/C, H_2, CH_3OH, 2h; (g) hexagonal magnetite, 1/1 $CH_3OH/CHCl_3$, 12h.

The size distribution of the resulting HMNPs was investigated by using the program package IMAGE/NIH, as described in reference 18. The resulting size distribution is shown in Figure 2, which is based on TEM results. Typical transmission electron micrographs are provided in the supplementary information section (SI).

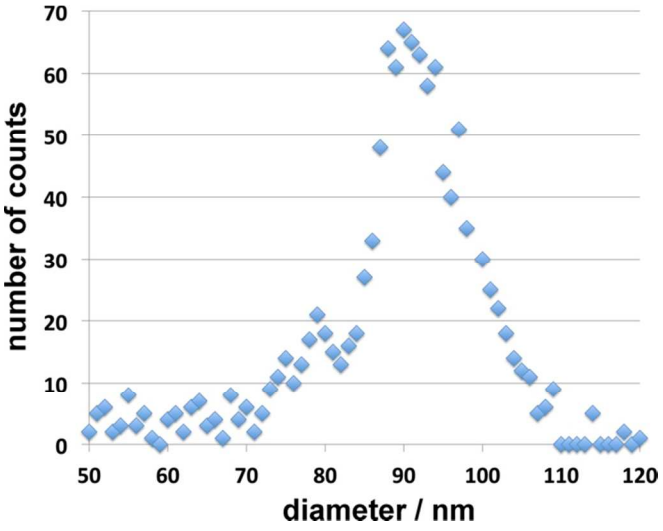

Figure 2. Diameters of the HMNPs as obtained by using IMAGE/NIH.[18] In a regular hexagon, the diameter is twice the edge length. The resulting main edge length is 45 ± 5 nm. The number of nanoparticles that are hexagons is > 85%. Note that the thickness of

the HMNPs cannot be determined by this method. It was estimated from TEM "shadow" at the edges.

3.4 HMNP Heating in an Alternating Magnetic Field

The heating ability of magnetic nanoparticles in an alternating magnetic field (AMF), measured in $Wg(Fe)^{-1}$ as specific absorption rates (SAR), is crucial for their performance in magnetic hyperthermia applications.[19] Larger values of SAR will permit lower administrated nanoparticle doses, as well as shorter and more effective hyperthermia treatments. This is of a special importance in cell-mediated cancer therapy, where stem cells[27] and defensive cells[28] are used to transport nanoparticles to tumors and metastases. It is noteworthy that SAR values depend on the size and shape of the nanoparticles.[29] We used an induction heater (Superior Induction Company, Pasadena, CA) to measure the SAR of hexagonal magnetite nanoprisms. The heater contains a copper coil, one inch in diameter with four turns, and is continuously cooled with cold water. The heater is operated with 5 kA/m field amplitude and 366 kHz frequency. To measure the temperature change, a fiber optic probe (Neoptix, Quebec, Canada) was used. When exposing a dispersion of 1.0 mg nanoparticles in 1.0 mL of water to the alternating magnetic field for 10 min, a temperature increase above 47 °C was observed. A control experiment carried out with 1.0 mL water alone showed only 3 °C temperature increase (Figure 3). The specific absorption rate (SAR) of hexagonal magnetite was calculated according to procedures described in reference 26 to be $765 \pm 12g\ Wg(Fe)^{-1}$.[30] It is noteworthy that the Hexagonal Magnetic Nanoprisms (HMNPs) exceed the SAR of Fe_3O_4 nanospheres when compared under the same A/C-magnetic field conditions by factors of 5 to 10. However, the SAR of HMNPs is only slightly higher than of nanocubes $740 \pm 10g\ Wg(Fe)^{-1}$

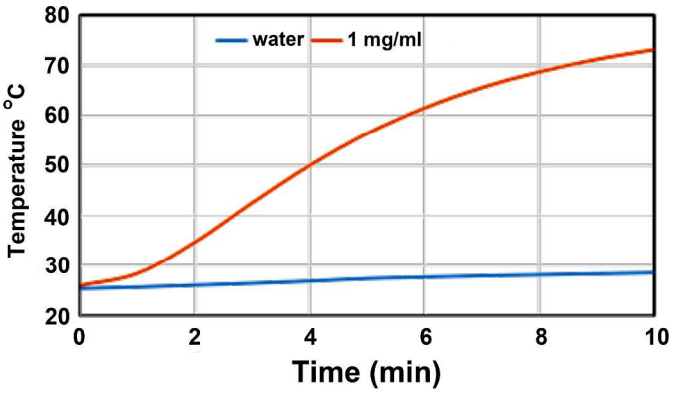

Figure 3. AMF heating of HMNP in water: (1 mg/mL), and 1 mL of DI water.

3.5 Shape-selective MF Hyperthermia Performance

The heating capabilities of hexagonal, cubic and spherical Fe_3O_4 nanoparticles of similar sizes at exactly the same concentration in water are summarized in Figure 4. Both, hexagonal and cubic Fe_3O_4 nanostructures demonstrated superior heating ability, compared to spherical nanoparticles. Martinez-Boubeta et al. suggested that the heating efficiency of nanoparticles in aqueous solution might be influenced by their aggregation into chains.[16] Face-to-face interaction between cubic nanoparticles favors this chain formation. Guardia et al. reported that iron oxide nanocubes (19±3 nm average diameter) possessed the highest SAR value in clinical conditions.[29b] Through carefully examination of the TEM's of hexagonal Fe_3O_4 nanoparticles, we observed that similar chain formation can occur in hexagonal Fe_3O_4 nanoparticles. There is strong evidence that the superior heating performance of both cubic and hexagonal nanostructures in AMF hyperthermia occurs from the same phenomenon, which is the formation of chains from individual nanostructures.

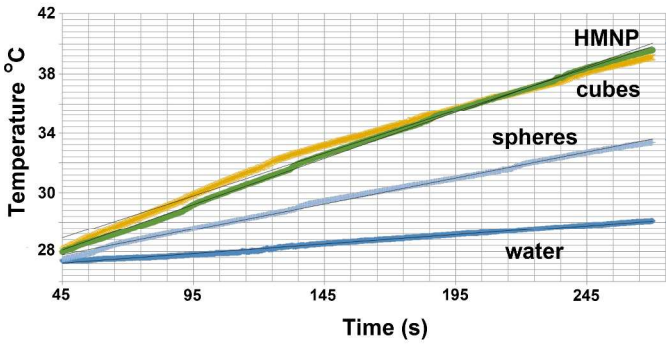

Figure 4. Heating performance of three Fe_3O_4 nanostructures (hexagonal nanoprisms (HMNP), cubes, and spheres) in water. HMPN and nanocubes used in these heating studies are shown in Figure 5. Fe_3O_4 spheres were synthesized as described in reference 31. The concentration of all three nanostructures was exactly 0.5 mg ml^{-1}.

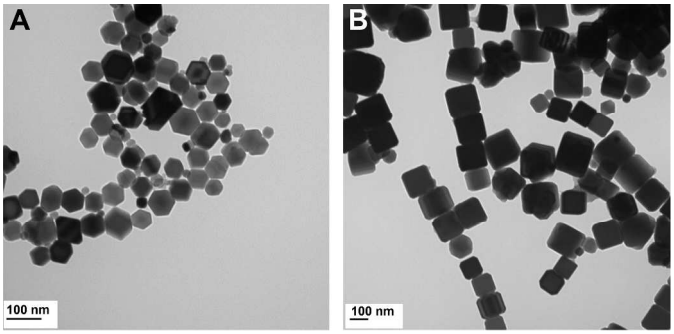

Figure 5. Chain formation by hexagonal Fe_3O_4 nanoprisms (HMNP, A) and Fe_3O_4 nanocubes (B)

3.6 Uptake of HMNPs by Monocyte/Macrophage-like Cells

Our groups have established that using tumor-homing cells as delivery vehicles to target magnetic nanoparticles to the tumor sites is a viable tool for the treatment of disseminated or deep-seated tumors.[27,28] Stem cells and defensive cells (e.g. neutrophils and monocytes/ macrophages) are known to infiltrate tumor sites.[32] Several recent studies have demonstrated the feasibility of delivering therapeutics to tumors using monocytes or macrophages.[33] In our previous research, we have reported that RAW264.7 cells (monocyte/macrophage-like cells, Mo/Ma ATCC TIB-71) can

specifically deliver magnetic nanoparticles to disseminated pancreatic tumors.[28] Here, we employed RAW264.7 cells to study the cellular uptake of hexagonal nanoprisms after exchange with hydrophilic ligand **4**. Removing HMNPs that were not taken up from Mo/Ma cells was challenging, because most of the cells and free HMNPs adhere to the culture flask, and are virtually impossible to wash away. To obtain accurate cell loadings, and cell viabilities of HMNPs, we lifted the Mo/Ma cells in 4°C 1 X PBS (phosphate buffered saline, pH = 7.4) containing 0.25% EDTA. Freed cells were collected by centrifugation, and then the cell pellet was re-suspended in PBS solution. Live and dead cells were counted in a hemocytometer utilizing trypan blue as exclusion dye.[20] Results indicate that the water-soluble HMNPs are well tolerated by RAW264.7 cells. Only less than 10% inhibition of cell proliferation

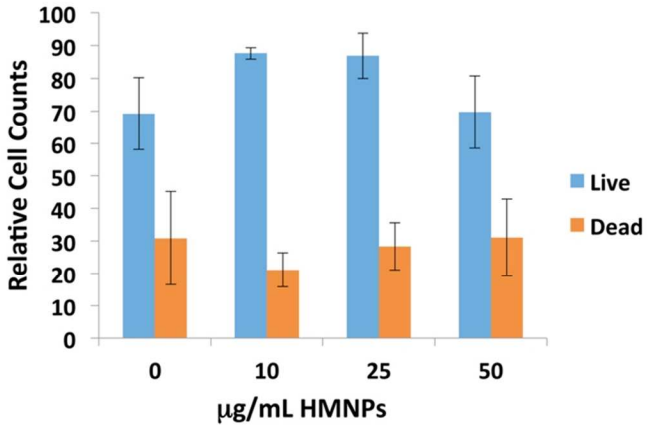

was found at 50 μg/mL iron concentration (Figure 6).

Figure 6. Relative cell counts of RAW264.7 cells, after incubation for 24 with different HMNPs concentration, followed by lifting in 4°C PBS/EDTA. Further explanations are provided in the text.

The lifted cells were re-plated. Figure 7 shows typical bright field images of HMNPs loaded RAW264.7 cells (5b, and 5c), which have been stained with Prussian blue to reveal the location of the HMNPs.

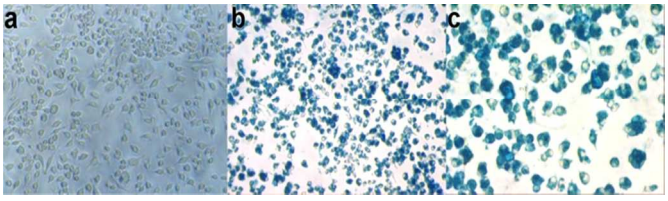

100% of the cells showed a blue stain when 50 μg/mL concentration of HMNPs was used, confirming effective loading of nanoparticles in these cells.

Figure 7. Bright field images of a) RAW264.7 cells alone (magnification 20×); b) Nanoparticle loaded RAW264.7 cells (magnification 20×) after Prussian blue staining; c) Nanoparticle loaded RAW264.7 cells (magnification 40×) after Prussian blue staining.

3.7 AMF Heating of Hexagonal RAW264.7 Cells after Uptake of Fe_3O_4 Nanoplatelets

It is of vital importance for cell based hyperthermia applications that the magnetic nanoparticles still can produce heat efficiently in an AC magnetic field after they have been taken up by delivery cells.

One million RAW264.7 cells in a 75 cm^2 flask were incubated with 10 mL of HMNPs dispersion (iron concentration: 40 μg/mL) for 24 hours. After washing with RPMI medium (twice) and 1 X PBS medium (twice) to remove free HMNPs, cells were then lifted by gentle scraping, and collected by centrifugation (1000 RPM) in 2.0 mL centrifuge tubes. The volume of the collected RAW264.7 cells and residual buffer was precisely set to 0.10 mL. Temperature increase as a function of time was compared between HMNP-loaded RAW264.7 cells and not loaded RAW264.7 cells (control) in an AMF (366 kHz, 5 kA/m). After 5min. of AMF exposure, the resulting temperature of the HMNP-loaded RAW264.7 cells was increased by 5.5 ± 1 °C, compared to the pellet formed from not loaded RAW264.7 cells. As Figure 8 indicates, minor inductive heating occurred in the absence of HMNPs.

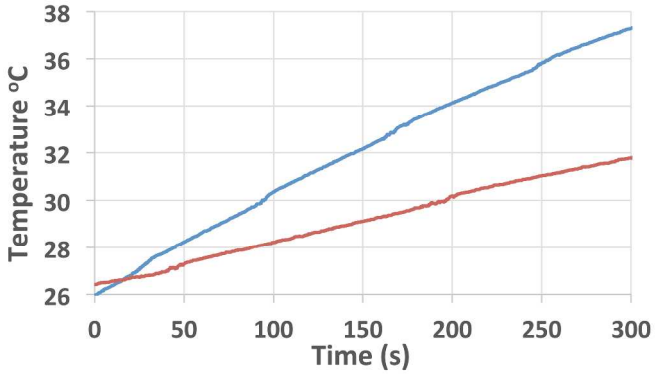

Figure 8. Temperature increase vs. time in two pellets containing 1 x 10^6 RAW264.7 cells each under AMF exposure (366 kHz, 5 kA/m). Blue line: RAW264.7 cells were loaded for 24h with HMNPs equivalent to 40 μg/mL Fe concentration. Orange line: not loaded RAW264.7 cells.

Assuming that the Specific Absorption Rate of the HMNPs is the same when taken up by RAW264.7 cells as in water, we have estimated from the observed A/C-magnetic heating the HMNP concentration that was taken up to 1.50 ± 0.04 x 10^{-5} g. This corresponds to 1.5 x 10^{-11} g per RAW264.7 cell and approx. 2.5 percent of the mass of HMNPs present in the culture flask during uptake. In our previous work, we had established the uptake of rod-like Fe/Fe_3O_4 nanoparticles (d = 20 ± 5 nm) featuring the same dopamine-based ligand **4**, that were obtained via sodium borohydride reaction of $FeCl_3$ in inverse micelles, to 2.12 ± 0.37 x 10^{-12} g per RAW264.7 cell.[28] Compared to these results, the uptake of the hexagonal nanoplatelets (45 ± 5 nm in edge length, estimated thickness of 5 to 6 nm) was increased by a factor of seven. It should be noted that the lower toxicity of the HMNPs permitted uptake for 24h, compared to 12h for the Fe/Fe_3O_4-nanorods. It is known from the extensive work on gold nanoparticles that endocytosis and phagocytosis are shape- and size selective uptake processes.[34] It is our hypothesis that this behaviour is not limited to gold

nanoparticles. According to the literature, there is a significant fraction of (gold) nanoparticles that will be surface bound by the free thiols that are present at the surface of defensive cells.[33] Our experiment cannot distinguish between internalized and surface-bound HMNPs, but both types will be transported by the cargo cell. Potentially, there is a minor fraction of "free" HMNPs that are collected together with the RAW264.7 cells. However, this fraction should be similar when loading the cells with both types of nanoparticles.

4. Conclusions

A facile method for preparing hexagonal Fe_3O_4 nanoplatelets under mild reaction conditions has been developed. After surface modification using a dopamine-based ligand, the nanoplatelets were readily taken up by RAW264.7 cells (monocyte/macrophage-like cells) displaying only minimal toxicity. The cell entrapped hexagonal nanoplatelets retained excellent heating ability under AMF (SAR > 750 Wg^{-1}). These findings demonstrate the feasibility of utilizing RAW264.7 cells as cancer targeting vehicles to specifically deliver the hexagonal Fe_3O_4 nanoplatelets to cancer sites in order to perform localized magnetic hyperthermia.

Acknowledgements

The authors acknowledge financial support from the National Science Foundation (ECCS #1128570, DMR #1242765, CBET #1337438) and from the Terry C. Johnson Cancer Center at Kansas State University.

Abbreviations

HMNPs: hexagonal magnetite nanoplatelets; PBS: phosphate buffered saline; $Fe(acac)_3$: iron(III)acetonylacetonate, AMF: alternating magnetic field; SAR: specific absorption rate

Notes and references

[a] Kansas State University, Department of Chemistry, 201 CBC Building, Manhattan, KS 66506, USA, hongwang@ksu.edu, sbossman@ksu.edu.
[b] Kansas State University, Department of Anatomy & Physiology, Coles Hall, Manhattan, KS 66506, USA.
[c] University of Kansas, Microscopy and Analytical Imaging Laboratory, Haworth Hall 1043, Lawrence, KS 66045, USA.
[d] Kansas State University, Department of Chemical Engineering, Durland Hall, Manhattan, KS 66506, USA.

Electronic Supplementary Information (ESI) available: [The coating of the Fe_3O_4 nanoplatelets with dopamine stealth ligand and the characterization techniques used are described in the SI section.]. See DOI: 10.1039/b000000x/

1 S. Sun, C. B. Murray, D. Weller, L. Folks and A. Moser, *Science*, 2000, **287**, 1989; D. Weller and M. F. Doerner, *Annu. Rev. Mater. Sci.*, 2000, **30**, 611; G. I. Frolov, *Tech. Phys.*, 2001, **46**, 1537; T. Hyeon, *Chem. Commun.*, 2003, 927; Y. K. Sung, B. W. Ahn and T. J. Kang, *J. Magn. Magn. Mater.*, 2012, **324**, 916.
2 J. W. M. Bulte and D. L. Kraitchman, *NMR Biomed.*, 2004, **17**, 484; W. J. M. Mulder, G. J. Strijkers, G. A. F. van Tilborg, A. W. Griffioen and K. Nicolay, *NMR Biomed.*, 2006, **19**, 142; J. Gao, G. Liang, J. S. Cheung, Y. Pan, Y. Kuang, F. Zhao, B. Zhang, X. Zhang, E. X. Wu and B. Xu, *J. Am. Chem. Soc.*, 2008, **130**, 11828.
3 C. Sestier, M. F. Da-Silva, D. Sabolovic, J. Roger and J. N. Pons, *Electrophoresis*, 1998, **19**, 1220; M. Racuciu, D. E. Creanga and G. Calugaru, *J. Optoelectron. Adv. Mater.*, 2005, **7**, 2859; V. Lobaz, R. N. Klupp Taylor and W. Peukert, *J. Colloid Interface Sci.*, 2012, **374**, 102.
4 J.-M. Nam, C. S. Thaxton and C. A. Mirkin, *Science,* 2003, **301**, 1884; D. K. Kim, M. Mikhaylova, F. H. Wang, J. Kehr, B. Bjelke, Y. Zhang, T. Tsakalakos and M. Muhammed, *Chem. Mater.*, 2003, **15**, 4343; S. Guo, D. Li, L. Zhang, J. Li and E. Wang, *Biomaterials*, 2009, **30**, 1881; H. Wang, T. B. Shrestha, M. T. Basel, R. K. Dani, G.-M. Seo, S. Balivada, M. M. Pyle, H. Prock, O. B. Koper, P. S. Thapa, D. Moore, P. Li, V. Chikan, D. L. Troyer and S. H. Bossmann, *Beilstein J. Nanotechnol.*, 2012, **3**, 444.
5 Y. R. Chemla, H. L. Grossman, Y. Poon, R. McDermott, R. Stevens, M. D. Alper and J. Clarke, *Proc. Natl. Acad. Sci. U. S. A.*, 2000, **97**, 14268; S. J. DeNardo, G. L. DeNardo, L. A. Miers, A. Natarajan, A. R. Foreman, C. Gruettner, G. N. Adamson and R. Ivkov, *Clin. Cancer Res.*, 2005, **11**, 7087.
6 A. H. Lu, E. L. Salabas and F. Schueth, *Angew. Chem., Int. Ed.*, 2007, **46**, 1222; J. Lee, Y. Lee, J. K. Youn, H. B. Na, T. Yu, H. Kim, S.-M. Lee, Y.-M. Koo, J. H. Kwak, H. G. Park, H. N. Chang, M. Hwang, J.-G. Park, J. Kim and T. Hyeon, *Small*, 2008, **4**, 143; C. Huang, H. Zhang, Z. Sun, Y. Zhao, S. Chen, R. Tao and Z. Liu, *J. Colloid Interface Sci.*, 2011, **364**, 298.
7 J. Rockenberger, E. C. Scher and A. P. Alivisatos, *J. Am. Chem. Soc.*, 1999, **121**, 11595; T. Hyeon, S. S. Lee, J. Park, Y. Chung and H. B. Na, *J. Am. Chem. Soc.*, 2001, **123**, 12798; S. Sun and H. Zeng, *J. Am. Chem. Soc.*, 2002, **124**, 8204; J. Park, E. Lee, N.-M. Hwang, M. Kang, S. C. Kim, Y. Hwang, J.-G. Park, H.-J. Noh, J.-Y. Kim, J.-H. Park and T. Hyeon, *Angew. Chem., Int. Ed.*, 2005, **44**, 2872.
8 M. V. Kovalenko, M. I. Bodnarchuk, R. T. Lechner, G. Hesser, F. Schaeffler and W. Heiss, *J. Am. Chem. Soc.*, 2007, **129**, 6352; D. Kim, N. Lee, M. Park, B. H. Kim, K. An and T. Hyeon, *J. Am. Chem. Soc.*, 2009, **131**, 454-455.
9 S. Palchoudhury, Y. Xu, J. Goodwin and Y. Bao, *J. Appl. Phys.*, 2011, **109**, 07E314/311.
10 L. M. Bronstein, J. E. Atkinson, A. G. Malyutin, F. Kidwai, B. D. Stein, D. G. Morgan, J. M. Perry and J. A. Karty, *Langmuir*, 2011, **27**, 3044.
11 Y. Wang and H. Yang, *Chem. Eng. J.*, 2009, **147**, 71.
12 L. Zhang, J. Wu, H. Liao, Y. Hou and S. Gao, *Chem. Commun.*, 2009, 4378.
13 J. Cheon, N.-J. Kang, S.-M. Lee, J.-H. Lee, J.-H. Yoon and S. J. Oh, *J. Am. Chem. Soc.*, 2004, **126**, 1950.
14 G. Zhen, B. W. Muir, B. A. Moffat, P. Harbour, K. S. Murray, B. Moubaraki, K. Suzuki, I. Madsen, N. Agron-Olshina, L. Waddington, P. Mulvaney and P. G. Hartley, *J. Phys. Chem. C*, 2011, **115**, 327.
15 G. Salazar-Alvarez, J. Qin, V. Sepelak, I. Bergmann, M. Vasilakaki, K. N. Trohidou, J. D. Ardisson, W. A. A. Macedo, M. Mikhaylova, M. Muhammed, M. D. Baro and J. Nogues, *J. Am. Chem. Soc.*, 2008, **130**, 13234.
16 C. Martinez-Boubeta, K. Simeonidis, A. Makridis, M. Angelakeris, O. Iglesias, P. Guardia, A. Cabot, L. Yedra, S. Estrade, F. Peiro, Z. Saghi, P. A. Midgley, I. Conde-Leboran, D. Serantes and D. Baldomir, *Sci. Rep.*, 2013, **3**, 1652.
17 Z. Li, J. F. Godsell, J. P. O'Byrne, N. Petkov, M. A. Morris, S. Roy and J. D. Holmes, *J. Am. Chem. Soc.*, 2010, **132**, 12540.
18 A. S. Perera, H. Wang, M. T. Basel, M. R. Pokhrel, P. S. Gamage, M. Kalita, S. Wendel, B. Sears, D. Welideniya, Y. Liu, C. Turro, D. L. Troyer and S. H. Bossmann, *Langmuir*, 2013, **29**, 308.
19 R. E. Rosensweig, *J. Magn. Magn. Mater.*, 2002, **252**, 370.
20 M. R. Melamed, L. A. Kamentsky and E. A. Boyse, *Science*, 1969, **163**, 285.

21 P.-H. Huang, C.-H. Lai and R. T. Huang, *J. Appl. Phys.*, 2005, **97**, 10C311/311.
22 Joint Committee on Powder Diffraction Standards (JCPDS) File No. 11-0614.
23 X.-L. Cheng, J.-S. Jiang, D.-M. Jiang and Z.-J. Zhao, *J. Phys. Chem. C*, 2014, **118**, 12588.
24 C. Li, R. Wei, Y. Xu, A. Sun and L. Wei, *Nano Res.*, 2014, **7**, 536.
25 W. J, Lyman, W. F. Reehl, D. H. Rosenblatt, D. H. Handbook of Chemical Property Estimation Methods. Environmental Behavior of Organic Compounds; American Chemical Society, 1990.
26 C. Xu, K. Xu, H. Gu, R. Zheng, H. Liu, X. Zhang, Z. Guo and B. Xu, *J. Am. Chem. Soc.*, 2004, **126**, 9938.
27 R. S. Rachakatla, S. Balivada, G.-M. Seo, C. B. Myers, H. Wang, T. N. Samarakoon, R. Dani, M. Pyle, F. O. Kroh, B. Walker, X. Leaym, O. B. Koper, V. Chikan, S. H. Bossmann, M. Tamura and D. L. Troyer, *ACS Nano*, 2010, **4**, 7093.
28 M. T. Basel, S. Balivada, H. Wang, T. B. Shrestha, G. M. Seo, M. Pyle, G. Abayaweera, R. Dani, O. B. Koper, M. Tamura, V. Chikan, S. H. Bossmann and D. L. Troyer, *Int. J. Nanomed.*, 2012, **7**, 297.
29 B. Mehdaoui, A. Meffre, J. Carrey, S. Lachaize, L.-M. Lacroix, M. Gougeon, B. Chaudret and M. Respaud, *Adv. Funct. Mater.*, 2011, **21**, 4573; P. Guardia, R. Di Corato, L. Lartigue, C. Wilhelm, A. Espinosa, M. Garcia-Hernandez, F. Gazeau, L. Manna and T. Pellegrino, *ACS Nano*, 2012, **6**, 3080.
30 The iron content of the hexagonal nanoprisms was determined by ICP to 66.1 percent by weight.
31 C. Hui, C. Shen, T. Yang, L. Bao, J. Tian, H. Ding, C. Li and H. J. Gao, *J. Phys. Chem. C*, 2008, **112**, 11336-11339.
32 G. Solinas, G. Germano, A. Mantovani and P. Allavena, *J. Leukocyte Biol.*, 2009, **86**, 1065; H. M. Strik, P. Hulper, B. Erdlenbruch, J. Meier, A. Kowalewski, B. Hemmerlein, R. Gold and M. Bahr, *Anticancer Res*, 2006, **26**, 865.
33 M. Matsui, Y. Shimizu, Y. Kodera, E. Kondo, Y. Ikehara and H. Nakanishi, *Cancer Sci.*, 2010, **101**, 1670; M. Muthana, A. Giannoudis, S. D. Scott, H.-Y. Fang, S. B. Coffelt, F. J. Morrow, C. Murdoch, J. Burton, N. Cross, B. Burke, R. Mistry, F. Hamdy, N. J. Brown, L. Georgopoulos, P. Hoskin, M. Essand, C. E. Lewis and N. J. Maitland, *Cancer Res.*, 2011, **71**, 1805; S.-K. Baek, A. R. Makkouk, T. Krasieva, C.-H. Sun, S. J. Madsen and H. Hirschberg, *J Neurooncol*, 2011, **104**, 439.
34 L. A. Dykman and N. G. Khlebtsov, *Chem. Rev.*, 2014, **114**, 1258.

For Table of Contents:

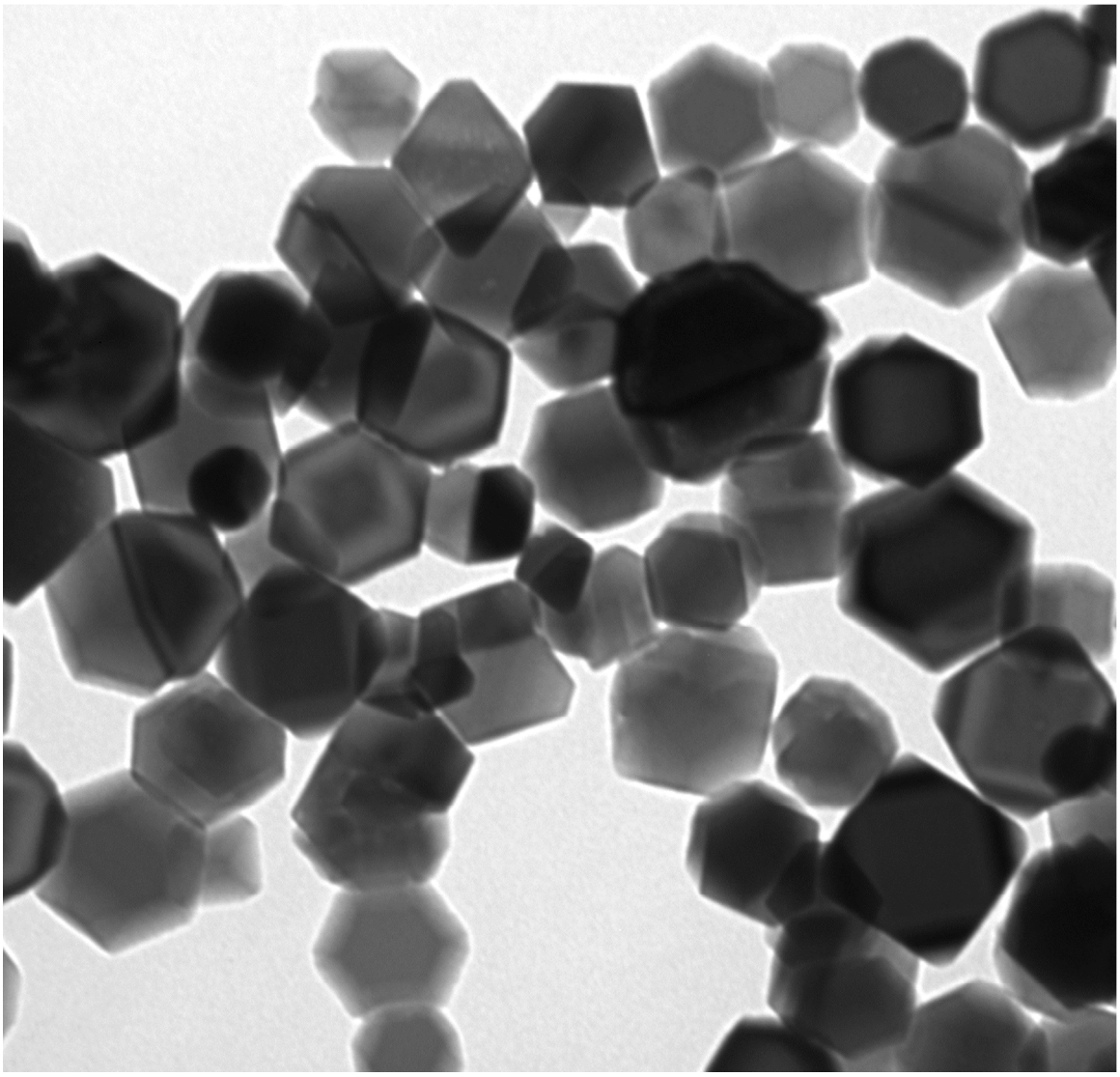

Synopsis:

Nearly perfect hexagonal Fe_3O_4 nanoplatelet structures, with edge length of 45 +/- 5 nm and thickness of 5 to 6 nm were synthesized from iron(III)acetonyl-acetonate using the dual ligand system oleic and stearic acid.